ACS Partner Journal

Journal of the American Society for Mass Spectrometry

pubs.acs.org/jasms

Research Article

Atheroma-Specific Lipids in *ldlr*$^{-/-}$ and *apoe*$^{-/-}$ Mice Using 2D and 3D Matrix-Assisted Laser Desorption/Ionization Mass Spectrometry Imaging

Jianhua Cao, Pieter Goossens, Marta Martin-Lorenzo, Frédéric Dewez, Britt S. R. Claes, Erik A. L. Biessen, Ron M. A. Heeren, and Benjamin Balluff*

Cite This: *J. Am. Soc. Mass Spectrom.* 2020, 31, 1825−1832

Read Online

ACCESS | Metrics & More | Article Recommendations | Supporting Information

ABSTRACT: Atherosclerosis is the major contributor to cardiovascular diseases. It is a spatially and temporally complex inflammatory disease, in which intravascular accumulation of a plethora of lipids is considered to play a crucial role. To date, both the composition and local distribution of the involved lipids have not been thoroughly mapped yet. Matrix-assisted laser desorption/ionization (MALDI) mass spectrometry imaging (MSI) enables analyzing and visualizing hundreds of lipid molecules within the plaque while preserving each lipid's specific location. In this study, we aim to identify and verify aortic plaque-specific lipids with high-spatial-resolution 2D and 3D MALDI-MSI common to high-fat-diet-fed low-density lipoprotein receptor deficient (*ldlr*$^{-/-}$) mice and chow-fed apolipoprotein E deficient (*apoe*$^{-/-}$) mice, the two most widely used animal models for atherosclerosis. A total of 11 lipids were found to be significantly and specifically colocalized to the plaques in both mouse models. These were identified and belong to one sphingomyelin (SM), three lysophosphatidic acids (LPA), four lysophosphatidylcholines (LPC), two lysophosphatidylethanolamines (LPE), and one lysophosphatidylinositol (LPI). While these lysolipids and SM 34:0;2 were characteristic of the atherosclerotic aorta plaque itself, LPI 18:0 was mainly localized in the necrotic core of the plaque.

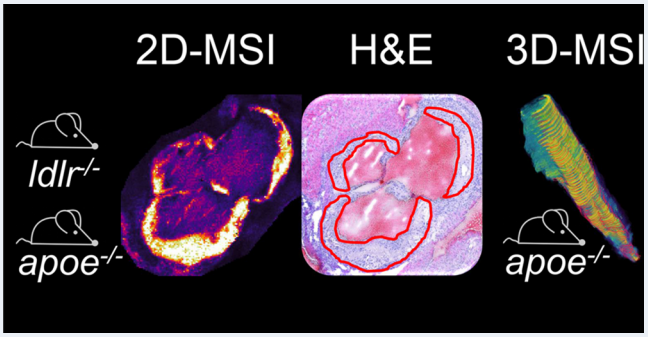

KEYWORDS: *atherosclerosis, mass spectrometry imaging, atheroma, plaque, LDLR, APOE*

INTRODUCTION

Cardiovascular diseases are the leading cause of death globally, and atherosclerosis is the major contributor. It is a chronic lipid-driven inflammatory disease characterized by atherosclerotic plaques formation in the arterial wall.[1−3]

Atherogenesis is initiated by endothelial dysfunction and activation followed by subendothelial lipoprotein accumulation and subsequent recruitment of immune cells. The resulting atheroma plaque consists of a lipid core and is covered by a plaque-stabilizing fibrous cap. Destabilizing factors such as cell death or calcification can result in rupture of this atheroma, thereby exposing the lipid content to the bloodstream, which can for instance lead to myocardial infarction or stroke.[1−3] Lipid composition, localization, and alteration along the arterial wall are considered to play a crucial role in the progression of atherosclerosis and the stability of the atheroma.[4] However, lipids constitute an extremely heterogeneous and abundant molecular class, which—combined with the spatial complexity of an atheroma—makes their *in situ* investigation extremely difficult.

In this context, mass spectrometry imaging (MSI) enables analyzing and visualizing hundreds of lipid molecules without labeling while each lipid's specific location in *ex vivo* biological tissue specimens is recorded.[5] Specifically, matrix-assisted laser desorption/ionization (MALDI)-MSI with its flexibility in spatial resolution (down to 10 μm) and in molecular classes (metabolites, proteins, lipids, glycans....) is increasingly applied in biomedical research. MALDI-MSI has demonstrated its unique capability of directly accessing a tissue's molecular content in an unlabeled manner in many studies,[6] among them several in the field of cardiovascular diseases.[7] In atherosclerotic research, however, MALDI-MSI remains an underexplored technique with only a few studies, which have so far have focused on the optimization of the experimental conditions and data processing.[8−10]

Previous studies of early atherosclerosis using MALDI-MSI in apolipoprotein E deficient (*apoe*$^{-/-}$) mice and in rabbits

Received: February 27, 2020
Revised: July 27, 2020
Accepted: July 27, 2020
Published: July 27, 2020

https://dx.doi.org/10.1021/jasms.0c00070
J. Am. Soc. Mass Spectrom. 2020, 31, 1825−1832

have already confirmed the presence of cholesterol in lipid-rich areas of the artery,[11] and have led to the identification of several lipid classes in the atheroma, respectively.[12] Nevertheless, these studies either suffer from a low number of samples or did not account for the volumetric complexity of atheromas.

In this study, we therefore address both issues using high-spatial-resolution 2-dimensional (2D) and three-dimensional (3D) MALDI-MSI to identify aortic plaque-specific lipids in two of the most widely studied mouse models for atherosclerosis. In a first phase, we investigate plaque-specific lipids in 15 low-density lipoprotein receptor deficient ($ldlr^{-/-}$) mice and four $apoe^{-/-}$ mice on a two-dimensional level involving several longitudinal replicates. Subsequently, we verify the volumetric plaque specificity of those lipids by 3D MALDI-MSI in an $apoe^{-/-}$ mouse to confirm the universal presence of these lipids along the plaque.

EXPERIMENTAL SECTION

Animal Models. Fifteen $ldlr^{-/-}$ male mice and six $apoe^{-/-}$ male mice were studied. Both models were on a C57BL/6 background to the 10th generation (Jackson Laboratory, Bar Harbor, ME, U.S.A.) and developed aortic atherosclerotic lesions under specific dietary conditions. Twelve-week-old $ldlr^{-/-}$ mice were fed a high-fat diet containing 16% fat and 0.15% cholesterol (AB Diets, Hope Farms, Woerden, The Netherlands) for 16 weeks. Forty-week-old $apoe^{-/-}$ mice had been fed a chow diet. All animals were housed under standard environmental conditions with a 12:12-h light-dark cycle. The mice were sacrificed and their aortic roots were fresh-frozen in OCT compound (Shandon, Veldhoven, The Netherlands) and stored at −80 °C until cryo-sectioning. All animal care and experimental procedures were in compliance with the Guidelines of the Maastricht University Animal Ethics Committee and the EU regulations for animal experimentation.

MSI Sample Preparation. Fifteen $ldlr^{-/-}$ and four $apoe^{-/-}$ mice aortic roots were sectioned at 7 μm thickness and perpendicular to the direction of blood flow using a cryomicrotome (Leica CM3050 S, Leica, Wetzlar, Germany), thaw-mounted onto indium−tin oxide (ITO) coated glass slides (CG-40IN-S115, Delta Technologies, Loveland, CO, U.S.A.), and stored at −80 °C until further analysis. For the $ldlr^{-/-}$ and $apoe^{-/-}$ mice, five sections were collected per mouse, each separated by 160 and 130 μm, respectively, to obtain a total of 115 tissue sections for a 2D analysis of the atheroma plaque.

For 3D MALDI-MSI of the whole aortic root from one $apoe^{-/-}$ mouse, 130 consecutive sections at 10 μm thickness were collected, where odd and even numbered sections were measured in negative and positive polarity, respectively. For posterior lipid identification, an additional $apoe^{-/-}$ mouse aortic root was sectioned at 10 μm thickness and thaw-mounted on membrane PEN slides (Leica Microsystems, Wetzlar, Germany).

All ITO slides were dried in a vacuum desiccator for 10 min and fiducial markers (Tipp-Ex, BIC, France) were applied to the ITO slide prior to matrix deposition. A 7 mg/mL norharmane matrix solution was prepared in 2:1 chloroform:-methanol (v:v) and homogeneously deposited onto the slides using an automated, temperature-controlled spraying system (TM-sprayer, HTX Technologies, Chapel Hill, NC, U.S.A.). Briefly, 15 layers were sprayed at 30 °C with a constant flow rate of 0.12 mL/min and at a speed of 1200 mm/min combined with 30 s drying time between each layer. Samples were measured immediately after matrix application.

2D and 3D MALDI-MSI Analysis. MSI lipid data within a mass range of m/z 400−2000 were acquired on a rapifleX MALDI Tissuetyper (Bruker Daltonik, Bremen, Germany) operating in reflector mode with 200 laser shots accumulated per pixel in both ion modes. For the 2D analysis, 115 sections were measured with a pixel size of 15 × 15 μm^2 (12 × 12 μm^2 beam scan region) as follows: 55 sections from 11 $ldlr^{-/-}$ animals and 20 sections from 4 $ldlr^{-/-}$ mice in negative and positive polarity, respectively, and 20 sections from 4 $apoe^{-/-}$ animals for each polarity. For the 3D $apoe^{-/-}$ analysis, 75 and 55 tissue sections were measured with a pixel size of 20 × 20 μm^2 (16 × 16 μm^2 beam scan region) in negative and positive ion mode, respectively. The instrument was calibrated using red phosphorus before the imaging measurement. Data acquisition and visualization were performed using FlexControl 4.0 and FlexImaging 5.0, respectively (both from Bruker Daltonik).

Histological Characterization. After MSI measurements, all ITO slides were washed with 70% methanol for 30 s to remove matrix before hematoxylin and eosin (H&E) staining. The samples were dried in a vacuum desiccator for 10 min, followed by rinsing in hematoxylin (Merck, Darmstadt, Germany) for 1 min, 10 min in tap water, 1 min in distilled water, and another 3 min in eosin (Merck, Darmstadt, Germany). Then, all sections were dehydrated in a graded ethanol series (70%, 2 × 96%, 2 × 100%, 2 min each) and finally rinsed for another 2 min in xylene. Coverslips were mounted onto the slides using a Tissue-Tek SCA 4764 Coverslipper (Sakura Finetek, The Netherlands). After air-drying overnight at room temperature, the H&E stained slides were scanned using a digital slide scanner (Mirax Desk, Zeiss, Jena, Germany) and coregistered in FlexImaging to the MSI data using the previously applied fiducial markers. Then, an expert in vascular pathology annotated plaque regions digitally in the scanned images.

Data Analysis and 3D Reconstruction. For an optimal spectral comparison, all data sets were first recalibrated using FlexAnalysis v3.4 (Bruker Daltonik). Recalibration for the negative ion mode data sets was performed in linear correction mode using m/z 885.6 as calibrant with a 1000 ppm peak assignment tolerance. Recalibration for the positive ion mode data sets was performed in quadratic mode using m/z 496.3, 524.4, 734.6, 758.6, and 782.6 as calibrants with a 500 ppm peak assignment tolerance. All recalibrated MSI data, coregistered H&E images, and plaque annotations were imported for every polarity separately to SCiLS Lab 2020a (Bruker Daltonik) for further analysis.

In SCiLS Lab, every spectrum was normalized to its root-mean-square value. The average spectra from each data set were exported to mMass 5.5.0[13] for peak-picking with the following parameters: (1) S/N ≥ 7.0, peak-picking height = 90%; (2) baseline correction precision: 35 for negative ion mode data sets and 5 for positive ion mode data sets with relative offset = 0; (3) Deisotoping: maximum charge = 1, isotope mass tolerance m/z = 0.1, isotope intensity tolerance = 70% and isotope mass shift = 0.0.

Matrix-derived peaks were removed via the loading plot of the principal component 2 (on tissue), resulting in 153 and 164 m/z species with a ± 200 ppm mass interval for the 2D data sets in positive and negative ionization modes, respectively.

https://dx.doi.org/10.1021/jasms.0c00070
J. Am. Soc. Mass Spectrom. 2020, 31, 1825−1832

Plaque specificity of m/z species was determined using the Pearson correlation coefficient in SCiLS lab with a minimum correlation coefficient of 0.4. 3D reconstruction and visualization of the $apoe^{-/-}$ MSI data was accomplished in SCiLS Lab by manually coregistering each pair of consecutive H&E images using prominent morphological features of the tissues as matched reference points.

Lipid Identification. Laser capture microdissection (Leica LMD7000, Leica Microsystems, Wetzlar, Germany) was used to accurately isolate the aortic plaques from 10 $apoe^{-/-}$ mouse aortic root sections to obtain the identities of the plaque-specific m/z signals as found by MALDI-MSI. Laser capture microdissection was performed using the following parameters: wavelength = 349 nm, power = 40, aperture = 11, speed = 10, specimen balance = 1, head current = 100%, and pulse frequency = 310 Hz. All plaque tissues were directly collected in an empty centrifuge tube.

The lipids from the collected plaque regions were extracted using 30 μL of matrix solution (7 mg/mL norharmane in 2:1 chloroform:methanol). The supernatant was spotted on an empty ITO slide for subsequent MALDI-MS/MS measurements using a Q-Exactive Hybrid Quadrupole-Orbitrap Mass Spectrometer (Thermo Fisher Scientific, Bremen, Germany) coupled to a MALDI source (Spectroglyph, Kennewick, U.S.A.). MS1 spectra from both mouse models were acquired within the mass range m/z 400−1000 in both ion modes with the following settings: mass resolution = 240 000 (@m/z 200), laser repetition rate = 1000 Hz, HPF pressure = 7.5 Torr, and velocity = 2 mm/sec. MS2 measurements were performed on supernatant from lipid extraction by using normalized collision energy in a range of 25−30 eV and a ± 0.5 Da isolation window while continuously moving the stage, with 25 scans averaged for each precursor. The online ALEX123 database (http://alex123.info/ALEX123/MS.php) was used for lipid assignments by matching the MS1 values and where available also the MS2 fragments with a mass tolerance of 3 and 5 ppm, respectively.

RESULTS

Plaque-Specific Lipids. To identify lipids specifically confined to the plaque, we analyzed atherosclerotic aortic roots from 15 high-fat diet fed $ldlr^{-/-}$ mice and four chow-diet fed $apoe^{-/-}$ mice using MALDI-MSI in both polarities. In total, 317 m/z species were detected in both data sets with a signal-to-noise ≥7. Spatial correlation analyses were used to find plaque colocalized m/z species with a Pearson coefficient ≥0.4 between the MSI images and the histology-based annotations of the atheroma plaque regions. This was done separately for the two mouse model data sets and resulted in 33 plaque-specific m/z species for the $ldlr^{-/-}$ mice (Figure 1a, Supplementary Table 1) and 43 for the $apoe^{-/-}$ mice (Figure 1a, Supplementary Table 2). Representative MSI images of plaque colocalized m/z species in $ldlr^{-/-}$ mice in negative (n = 10) and positive (n = 23) ion mode are shown in Supplementary Figures 1 and 2, respectively. MSI images of plaque-colocalized m/z species in the $apoe^{-/-}$ mice in negative (n = 24) and positive (n = 19) ion modes are shown in the Supplementary Figures 3 and 4, respectively.

Both mouse models had 25 plaque-specific m/z species in common (Figure 1b). All of these, except m/z 496.6, were identified using high-mass resolution MS1 and M2 experiments and belong to 18 lipids, as detailed in Table 1. All MS/MS spectra are shown in Supplementary Figures 5−22. Five

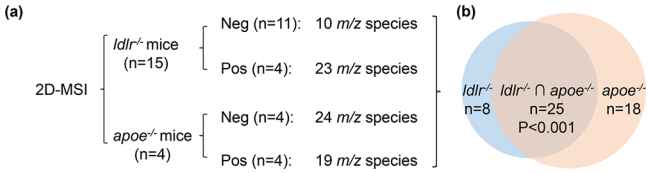

Figure 1. Study design and results of common plaque-specific lipids. Two-dimensional (2D) MALDI mass spectrometry imaging (MSI) was performed on aortic roots from 15 $ldlr^{-/-}$ and four $apoe^{-/-}$ mice in positive (Pos) and negative (Neg) ionization modes, which resulted in 33 and 43 m/z species spatially correlated to the plaque for the $ldlr^{-/-}$ and $apoe^{-/-}$ mouse models, respectively (a). The overlap of these plaque-specific m/z species between both mouse models was 25, which was statistically significant (P < 0.001) using a hypergeometric test (b).

m/z species were found to correspond to mixtures of lipids based on MS1 and MS2 levels, leaving 11 unambiguously identified lipids (Table 1), comprising 1 sphingomyelin (SM) and 10 lysolipids. Lysolipids correspond to 3 lysophosphatidic acids (LPA), 4 lysophosphatidylcholines (LPC), 2 lysophosphatidylethanolamines (LPE), and 1 lysophosphatidylinositol (LPI).

Representative MSI images of plaque-co-localized lipids LPA 16:0 and LPC 18:2 in both mouse models in negative and positive ion mode are shown in Figures 2 and 3, respectively. These images show that the *in situ* localization and plaque-correlation of these common lipids are very similar in both animal models (Supplementary Figures 1−4). Interestingly, we observed m/z 599.3 (LPI 18:0) to be nonhomogeneously distributed within the plaque. Using annotations of characteristic plaque features, we found LPI 18:0 to be specifically localized in the necrotic core region (Figure 4). This was observed consistently in both animal models.

Volumetric Evaluation of Plaque-Specific Lipids. To investigate the volumetric distribution of the 11 plaque-specific lipids along the plaque's length, 55 and 75 20 μm-spaced tissue sections from an aortic root of one $apoe^{-/-}$ mouse were measured by MSI in positive and negative ion mode, respectively. Spatial correlation analysis to plaque annotations across all sections of the 3D MSI data was performed for the 25 m/z species belonging to the 11 lipids of interest. Twenty-two m/z species (Supplementary Table 3), which represent 10 unambiguously identified lipids, were found to have a correlation coefficient of at least 0.4 across the whole plaque. This analysis hence confirmed that 10 (LPA 18:1, LPA 20:1, LPE O-18:1, LPE 18:0, LPC 16:0, LPC 18:0, LPC 18:1, LPC 18:2, LPI 18:0, and SM 34:0;2) out of the 11 lipids can be considered plaque-specific in all three dimensions of the plaque. The 3D spatial distributions of selected lipids along the bloodstream direction are shown in longitudinal view in Figure 5a, where the signals belonging to m/z 480.3 (LPE 18:0/LPC 16:0) and m/z 599.3 (LPI 18:0) delineate the plaque and necrotic core areas, respectively. Supplementary Video 1 shows the 3D reconstruction of m/z 480.3 (LPE 18:0/LPC 16:0) in rotation. Furthermore, the spatial correlation analysis was performed individually for every section of the 3D MSI data set to obtain a more detailed view on the specificity of these lipids for plaque and necrotic core areas along the third dimension. Figure 5b shows the variation of the correlation coefficients of m/z 480.3 (LPE 18:0/LPC 16:0) to the plaque area and of m/z 599.3 (LPI 18:0) to the necrotic core area, and Supplementary Figure 23 shows the remaining lipids.

https://dx.doi.org/10.1021/jasms.0c00070
J. Am. Soc. Mass Spectrom. 2020, 31, 1825−1832

Table 1. Twenty-Five Plaque-Specific m/z Species in Both, $ldlr^{-/-}$ and $apoe^{-/-}$, Mouse Models

observed m/z by TOF	Pearson correlation coefficient		observed m/z by Orbitrap	lipid assignment	MS experiment level for ID	ion mode	mass error (in ppm)
	$ldlr^{-/-}$	$apoe^{-/-}$					
409.3	0.47	0.61	409.2366	$[LPA\ 16:0-H]^-$	MS1	NEG	+1.3
459.2	0.50	0.46	459.2476	$[LPA\ 18:1+Na]^+$	MS1	POS	−1.3
463.3	0.41	0.54	463.2839	$[LPA\ 20:1-H]^-$	MS1	NEG	+1.9
464.3	0.44	0.59	464.3142	$[LPE\ O\text{-}18:1-H]^-$	MS1	NEG	−1.0
480.3	0.52	0.62	480.3099	$[LPE\ 18:0-H]^-$/ $[LPC\ 16:0-CH_3]^-$	MS2	NEG	+0.6
482.3	0.55	0.50	482.3600	$[LPC\ O\text{-}16:0+H]^+$/ $[LPE\ O\text{-}19:0+H]^+$	MS1	POS	−1.0
487.3	0.47	0.44	487.2790	$[LPA\ 20:1+Na]^+$	MS1	POS	−1.0
496.3	0.58	0.62	496.3398	$[LPC\ 16:0+H]^+$	MS2	POS	+0.0
496.6	0.60	0.49	/	/	/	POS	/
506.3	0.43	0.41	506.3257	$[LPC\ 18:1\text{-}CH_3]^-$/$[LPE\ 20:1-H]^-$	MS1	NEG	+1.0
510.4	0.59	0.55	510.3554	$[LPC\ 17:0+H]^+$/$[LPE\ 20:0+H]^+$	MS1	POS	+0.0
518.3	0.59	0.63	518.3216	$[LPC\ 16:0+Na]^+$	MS2	POS	−0.2
520.3	0.63	0.63	520.3400	$[LPC\ 18:2+H]^+$	MS2	POS	+0.4
522.4	0.56	0.59	522.3557	$[LPC\ 18:1+H]^+$	MS2	POS	+0.6
524.4	0.45	0.52	524.3717	$[LPC\ 18:0+H]+$	MS2	POS	+1.1
534.3	0.57	0.57	534.2951	$[LPC\ 16:0+K]^+$	MS2	POS	−0.9
538.4	0.43	0.53	538.3862	$[LPC\ 19:0+H]^+$/ $[LPE\ 22:0+H]^+$	MS1	POS	−1.0
542.4	0.58	0.57	542.3213	$[LPC\ 18:2+Na]^+$	MS1	POS	−0.8
544.4	0.59	0.57	544.3389	$[LPC\ 18:1+Na]^+$	MS2	POS	+2.8
546.4	0.56	0.49	546.3540	$[LPC\ 18:0+Na]^+$	MS2	POS	+1.8
560.3	0.49	0.45	560.3123	$[LPC\ 18:1+K]^+$	MS2	POS	+0.0
562.3	0.49	0.49	562.3278	$[LPC\ 18:0+K]^+$	MS2	POS	+0.0
599.3	0.41	0.52	599.3216	$[LPI\ 18:0-H]^-$	MS2	NEG	+2.4
689.6	0.42	0.53	689.5620	$[SM\ d18:0\_16:0\text{-}CH_3]^-$	MS2	NEG	+0.7
727.6	0.40	0.44	727.5731	$[SM\ 34:0;2+Na]^+$	MS2	POS	+1.0

DISCUSSION

In this study we aimed to identify aortic plaque-specific lipids by high-spatial-resolution MALDI-MSI and 3D MALDI-MSI in high-fat-diet-fed low-density lipoprotein receptor deficient ($ldlr^{-/-}$) mice and chow-fed apolipoprotein E deficient ($apoe^{-/-}$) mice. These two mouse models are the most-widely investigated mouse models in cardiovascular research. As the pathogenesis and manifestation of atherosclerosis in both models is slightly different,[14] identifying common molecular mechanisms harbors the potential to better understand key processes in the development of atherosclerosis.

Previous studies have already used MALDI mass spectrometry imaging to study the lipidic composition of the atheroma plaque in human[9,10,15] or $apoe^{-/-}$ mouse model samples.[11] We could confirm the observation of most LPCs (Table 1), several ceramide species (Supplementary Table 2), cholesteryl esters (CEs), and oxysterols to be localized in the plaque (Supplementary Figures 24−25), although the latter two did not pass our peak picking thresholds. Our study complements these results by confirming the presence of those lipids also in $ldlr^{-/-}$ mice and adding to that list other plaque-specific lysolipids such as several LPAs, LPEs, and LPIs. Using a higher spatial resolution (15 μm) than previous studies allowed us to spot certain lipid species in subcompartments of the plaque. Furthermore, all lipid identifications are based on high-mass resolution MS1 ($R_{observed}$ ∼ 120 000@m/z 800) or MS2 measurements, thereby providing a higher certainty of the molecular identities.

Using an additional 3D approach allowed us to investigate the specificity of the detected lipids along the third dimension of the plaque. That we analyzed the entire plaque can be seen in Figure 5b where the plaque's hill-shaped topography is shown on the basis of the size of the annotated plaque areas in each section. This analysis also shows that the lipids' spatial specificity remains stable along the z-direction of the plaque and is independent of the blood flow direction.

Most of our identified lipids are lysophospholipids, including LPA, LPC, LPE, and LPI species, suggesting that in both mouse models the plaque lipid pool is mainly composed of different lysophospholipids. Lysophospholipids are bioactive lipid-derived metabolic intermediates in biodegradation of membrane phospholipids and act as extracellular mediators involved in development and progression of atherosclerosis.[16]

LPCs are major plasma lipids that are highly enriched in oxidized low-density lipoprotein (oxLDL), a highly pro-atherogenic modified lipoprotein.[17] Although a recent MSI study by Diehl et al. has shown the presence of LPCs at the highest vulnerable plaque regions in humans,[15] to the best of our knowledge, we have shown for the first time that LPC 16:0, LPC 18:0, LPC 18:1, and LPC 18:2 are specifically and exclusively located in the atheroma plaque and not in the rest of the artery in both mouse models. Interestingly, these lipid species have been related with a higher incidence of cardiovascular diseases in serum and plasma samples,[18−20] where serum levels have been related to different grades of calcification in coronary artery disease.[21] Serum LPC 18:2 has also been proposed as myocardial infarction biomarker.[22] This

https://dx.doi.org/10.1021/jasms.0c00070
J. Am. Soc. Mass Spectrom. 2020, 31, 1825−1832

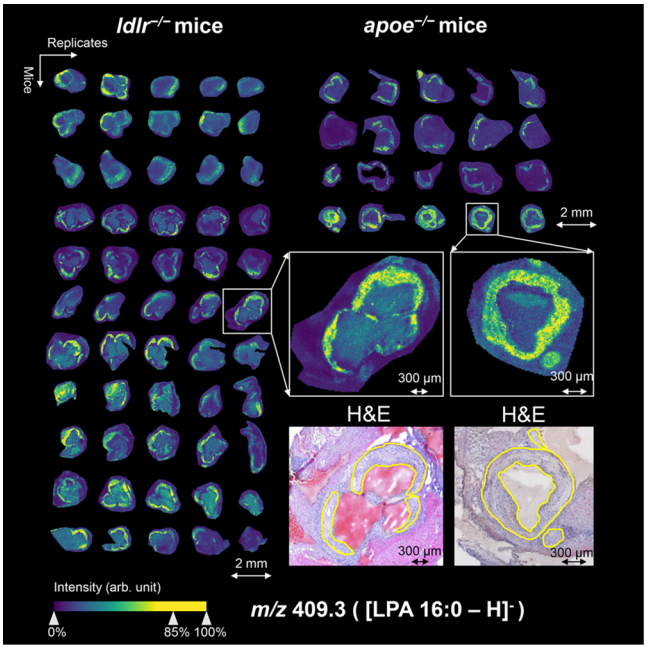

Figure 2. Visualization of m/z 409.3 (LPA 16:0) in aortic roots of $ldlr^{-/-}$ mice and $apoe^{-/-}$ mice in negative ion mode. On the left, the MALDI mass spectrometry imaging visualization of LPA 16:0 is shown for 55 different tissue sections of 11 $ldlr^{-/-}$ mice, and on the right for 20 different tissue sections of 4 $apoe^{-/-}$ mice, showing specific plaque localization in all aortas. Magnifications of two representative tissue sections are depicted on the lower right together with their coregistered, hematoxylin and eosin (H&E)-stained images (plaque circumferences are indicated in yellow).

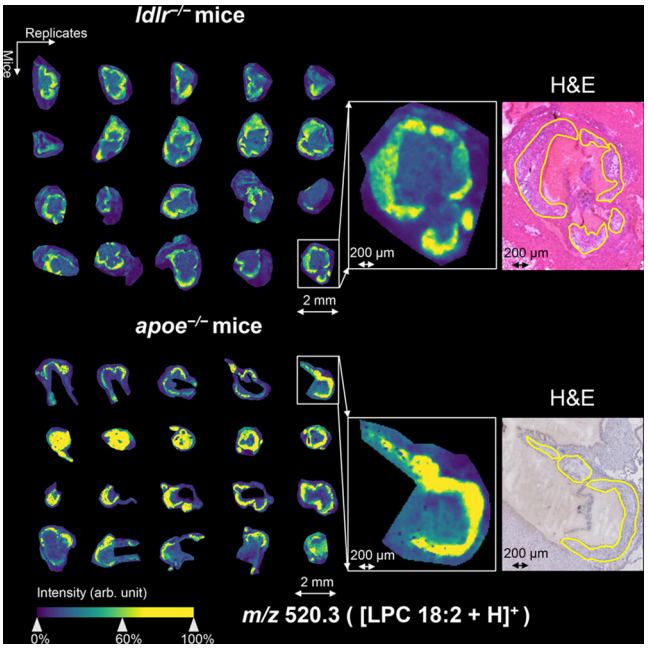

Figure 3. Visualization of m/z 520.3 (LPC 18:2) in aortic roots of $ldlr^{-/-}$ mice and $apoe^{-/-}$ mice in positive ion mode (with weak denoising). On the left, the location of LPC 18:2 in 40 different tissue sections of four mice from every mouse model is shown as detected by MALDI mass spectrometry imaging. Magnifications of selected tissue sections and their coregistered, hematoxylin and eosin (H&E)-stained images are shown in the right-hand side (plaque circumferences are indicated in yellow).

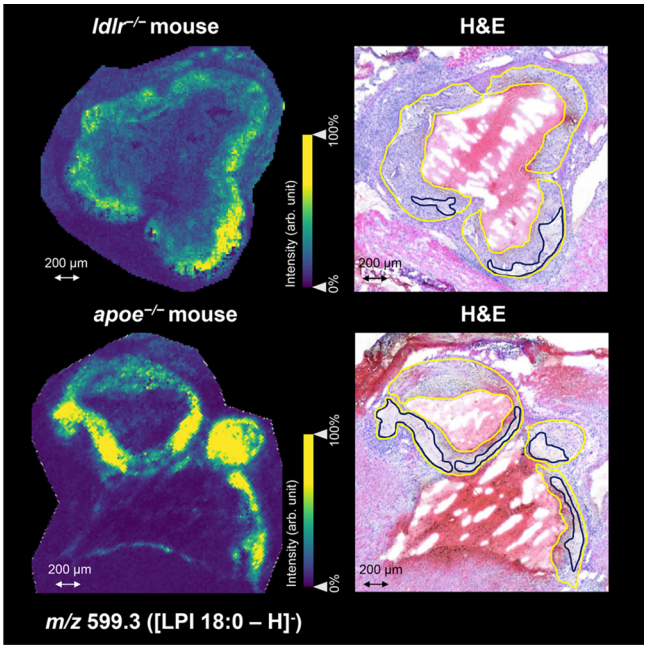

Figure 4. Visualization of m/z 599.3 (LPI 18:0) in aortic roots of $apoe^{-/-}$ and $ldlr^{-/-}$ mouse in negative ion mode. On the left, the location of LPI 18:0 is shown as detected by MALDI mass spectrometry imaging in both mouse models. On the right, the coregistered hematoxylin and eosin (H&E)-stained images demonstrate that LPI 18:0 is particularly confined to the necrotic core regions within the plaques (plaque and necrotic core circumferences are indicated in yellow and dark blue, respectively).

makes an interesting link between highly abundant blood circulating lipids and plaque-specific lipids that should be further studied.

Several LPA species including 16:0, 18:1, and 20:1 were detected in the plaques of both mouse models. The relation of LPAs with atherosclerosis and specifically with the atheroma plaque has been studied earlier by us[23,24] and others[25] concluding that there is strong evidence that LPAs participate in formation and rupture of the plaque.[23,25] LPAs have been previously found to accumulate in the central atheroma in human and mouse plaques.[26] Indeed, LPA 16:0 and LPA 18:1 have been detected before in carotid mice plaques.[24] However, LPA 20:1 has not been related before to atherosclerosis, neither has it been specifically located within the atheroma plaque.

The presence of both, LPAs and LPCs, has been related with highly vulnerable plaques and poor prognosis.[15,26] It has been suggested that plaque rupture exposes these lysophospholipids, which in turn activate platelets. This results in an increase of aggregates and thrombogenic potential, leading to a fatal event. In the present work, we identified specific LPAs (LPA 16:0, 18:1, 20:1) and LPCs (LPC 16:0, 18:0, 18:1, 18:2) in the plaque area. The specific characterization of these LPAs/LPCs is a step forward because there is evidence that the fatty acid composition and the linkage of the fatty acid to the glycerol backbone may affect this platelet activation[27] and subsequently affect the stability of the plaque.

LPEs and LPIs in atherosclerosis have been less studied than other lysolipids, which might be attributed to their lower abundance. Different species of LPE have been detected in plasma in association with incident cardiovascular disease but without statistical significance.[20] We have identified and

https://dx.doi.org/10.1021/jasms.0c00070
J. Am. Soc. Mass Spectrom. 2020, 31, 1825−1832

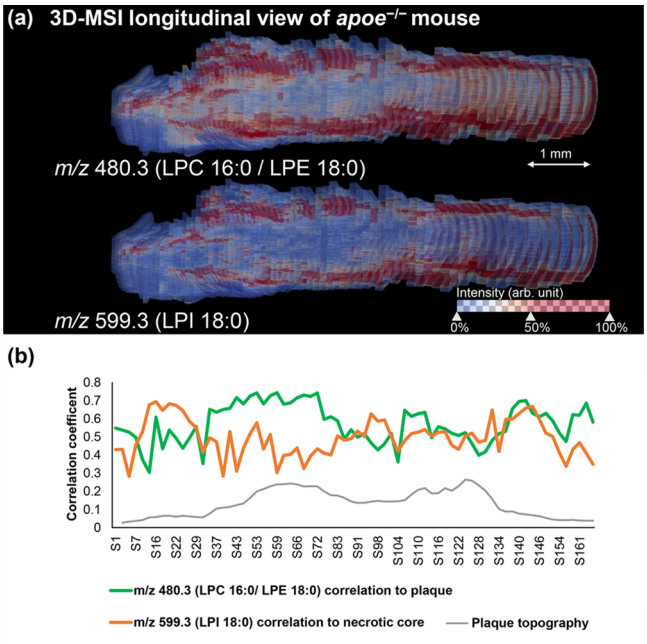

Figure 5. Three-dimensional longitudinal visualization of the plaque-specific lipids m/z 480.3 (LPE 18:0/LPC 16:0) and m/z 599.3 (LPI 18:0) as detected by 3D MALDI mass spectrometry imaging in an aortic root of an $apoe^{-/-}$ mouse (a). Spatial correlation analysis was performed for m/z 480.3 (LPE 18:0/LPC 16:0) on the annotated plaque area and for m/z 599.3 (LPI 18:0) on the annotated necrotic core area, respectively, on a section-by-section basis. This allows showing the variation of the correlation of two lipids to the respective annotations along the z-direction of the plaque (b). The blood flow direction is from left to right.

correlated the specific presence of LPE 18:0 and LPE O-18:1 in the atheroma plaque. In this respect, it is also the first time that LPI 18:0 has been found particularly localized in the necrotic core of plaques in both mouse models, but its role in necrosis is presently unknown. However, we can hypothesize that the presence of LPI in the necrotic core is related to poor prognosis. The necrotic core is not only one of the most vulnerable plaque components, but also appears to be the most thrombogenic component. Moreover, high levels of LPI have been related with a poor outcome in acute myocardial infarction.[28] Nevertheless, the specific role of this LPI in necrosis still has to be explored with other techniques.

The high levels of the lysolipids identified here in the plaques can be related with different mechanisms. On the one hand, LPI, LPE, and LPC are generated from their correspondent phospholipid (i.e., phosphatidylinositol, phosphatidylethanolamine, and phosphatidylcholine).[29,30] On the other hand, LPA is mainly produced from LPC by autotaxin.[25] In that line, LPA accumulation has been related to an increase of LPC as precursor of LPA.[24] The high abundance of LPC 16:0 and 18:1, LPA 16:0 and 18:1 suggests an intraplaque LPA production which would be in agreement with previous findings.[23,24] Besides, the participation of minor lysophospholipids may be also involved in the *in situ* synthesis[25], and in this sense the presence of LPA 16:0 together with LPC 16:0 and LPA 18:1 together with LPC 18:1 could be related with this lysolipids interchange mechanism. However, more experiments and research on this *in situ* formation or direct accumulation should be done.

Another lipid class that has been associated with plaque is sphingomyelin (SM).[4,10,31] SMs are a subgroup of sphingolipids, which are formed via derivation of palmitoyl-CoA and L-serine.[32] We detected two SM species (SM 34:0;2 and SM 34:1;2) in both ionization modes of which only SM 34:0;2 was significantly localized in plaques of both mouse models (Supplementary Figure 26). Interestingly, no other MSI study has ever reported SM 34:0;2 to be plaque specific. While in our study SM 34:1;2 was only found in plaques of $apoe^{-/-}$ mice (correlation coefficient >0.5) and to lower extent in $ldlr^{-/-}$ mice (correlation coefficient = 0.35), others have found this lipid in human coronary arteries.[10,31] In plasma, several studies have found SM levels in human plasma to be indicative of coronary heart diseases.[32,33] The role of SMs has been investigated in animal models, which showed that atherosclerotic lesions progressed with a SM-rich diet.[34]

The use of mouse models limits the certainty by which results can be translated directly to the human disease condition. In this study, we have focused our analysis and discussion on the commonalities of two of the most common and understood mouse models in atherosclerosis. The fact that our results are consistent across the two different models is promising and indicates that they could be extended to the study of human plaque and plasma samples.

CONCLUSIONS

2D and 3D MALDI mass spectrometry imaging was used to comprehensively investigate the lipid profile of murine atherosclerotic plaque tissue, in two distinct mouse models using technical and biological replicates. The study identified 11 plaque-specific lipids present in both atherosclerotic mouse models. All the results presented in this study suggest that lysolipids and sphingomyelins are integral constituents of the plaque in atherosclerosis. More specifically, LPI 18:0 was concentrated in the necrotic core of plaques. These novel results unravel the molecular complexity of the atherosclerotic plaque enhancing not only our understanding of plaque composition but also the identification of potential plaque lipid species related with plaque stability.

ASSOCIATED CONTENT

Supporting Information

The Supporting Information is available free of charge at https://pubs.acs.org/doi/10.1021/jasms.0c00070.

Additonal data as mentioned in the text (PDF)

3D reconstruction of m/z 480.3 (LPE 18:0/LPC 16:0) in rotation (AVI)

AUTHOR INFORMATION

Corresponding Author

Benjamin Balluff − *Maastricht Multimodal Molecular Imaging Institute (M4I), Maastricht University, 6200 MD Maastricht, The Netherlands;* orcid.org/0000-0003-0351-240X; Email: b.balluff@maastrichtuniversity.nl

Authors

Jianhua Cao − *Maastricht Multimodal Molecular Imaging Institute (M4I), Maastricht University, 6200 MD Maastricht, The Netherlands*

Pieter Goossens − *Maastricht UMC+, Pathology Department, Cardiovascular Research Institute Maastricht (CARIM), 6202 AZ Maastricht, The Netherlands*

Marta Martin-Lorenzo − *Maastricht Multimodal Molecular Imaging Institute (M4I), Maastricht University, 6200 MD Maastricht, The Netherlands; Immunology Department, IIS-Fundacion Jimenez Diaz-UAM, 28040 Madrid, Spain*

Frédéric Dewez − *Maastricht Multimodal Molecular Imaging Institute (M4I), Maastricht University, 6200 MD Maastricht, The Netherlands; Mass Spectrometry Laboratory (MSLab), University of Liège, B-4000 Liège, Belgium*

Britt S. R. Claes − *Maastricht Multimodal Molecular Imaging Institute (M4I), Maastricht University, 6200 MD Maastricht, The Netherlands*

Erik A. L. Biessen − *Maastricht UMC+, Pathology Department, Cardiovascular Research Institute Maastricht (CARIM), 6202 AZ Maastricht, The Netherlands*

Ron M. A. Heeren − *Maastricht Multimodal Molecular Imaging Institute (M4I), Maastricht University, 6200 MD Maastricht, The Netherlands;* orcid.org/0000-0002-6533-7179

Complete contact information is available at: https://pubs.acs.org/10.1021/jasms.0c00070

Author Contributions

The manuscript was written through contributions of all authors.

Notes

The authors declare no competing financial interest.

■ ACKNOWLEDGMENTS

This work was funded by the China Scholarship Council (No. 201706040068) and by the Dutch Province of Limburg through the LINK program. BB, MML and FD also acknowledge the financial support of the European Union (ERA-NET TRANSCAN 2; Grant No. 643638). MML acknowledges the financial support of the Conserjeria de Educacion, Juventud y Deporte de la Comunidad de Madrid (contract: 2018-T2/BMD-11561).

■ REFERENCES

(1) Lusis, A. J. Atherosclerosis. *Nature* **2000**, *407*, 233−241.
(2) Libby, P. Inflammation in atherosclerosis. *Arterioscler., Thromb., Vasc. Biol.* **2012**, *32*, 2045−2051.
(3) Badimon, L.; Vilahur, G. Thrombosis formation on atherosclerotic lesions and plaque rupture. *J. Intern. Med.* **2014**, *276*, 618−632.
(4) Martin-Lorenzo, M.; Balluff, B.; Maroto, A. S.; Carreira, R. J.; van Zeijl, R. J.; Gonzalez-Calero, L.; de la Cuesta, F.; Barderas, M. G.; Lopez-Almodovar, L. F.; Padial, L. R.; McDonnell, L. A.; Vivanco, F.; Alvarez-Llamas, G. Molecular anatomy of ascending aorta in atherosclerosis by MS Imaging: Specific lipid and protein patterns reflect pathology. *J. Proteomics* **2015**, *126*, 245−251.
(5) Chughtai, K.; Heeren, R. M. Mass spectrometric imaging for biomedical tissue analysis. *Chem. Rev.* **2010**, *110*, 3237−3277.
(6) Vaysse, P. M.; Heeren, R. M. A.; Porta, T.; Balluff, B. Mass spectrometry imaging for clinical research - latest developments, applications, and current limitations. *Analyst* **2017**, *142*, 2690−2712.
(7) Mezger, S. T. P.; Mingels, A. M. A.; Bekers, O.; Cillero-Pastor, B.; Heeren, R. M. A. Trends in mass spectrometry imaging for cardiovascular diseases. *Anal. Bioanal. Chem.* **2019**, *411*, 3709−3720.
(8) Martin-Lorenzo, M.; Balluff, B.; Sanz-Maroto, A.; van Zeijl, R. J.; Vivanco, F.; Alvarez-Llamas, G.; McDonnell, L. A. 30mum spatial resolution protein MALDI MSI: In-depth comparison of five sample preparation protocols applied to human healthy and atherosclerotic arteries. *J. Proteomics* **2014**, *108*, 465−468.
(9) Patterson, N. H.; Doonan, R. J.; Daskalopoulou, S. S.; Dufresne, M.; Lenglet, S.; Montecucco, F.; Thomas, A.; Chaurand, P. Three-dimensional imaging MS of lipids in atherosclerotic plaques: Open-source methods for reconstruction and analysis. *Proteomics* **2016**, *16*, 1642−1651.
(10) Visscher, M.; Moerman, A. M.; Burgers, P. C.; Van Beusekom, H. M. M.; Luider, T. M.; Verhagen, H. J. M.; Van der Steen, A. F. W.; Van der Heiden, K.; Van Soest, G. Data Processing Pipeline for Lipid Profiling of Carotid Atherosclerotic Plaque with Mass Spectrometry Imaging. *J. Am. Soc. Mass Spectrom.* **2019**, *30*, 1790−1800.
(11) Zaima, N.; Sasaki, T.; Tanaka, H.; Cheng, X. W.; Onoue, K.; Hayasaka, T.; Goto-Inoue, N.; Enomoto, H.; Unno, N.; Kuzuya, M.; Setou, M. Imaging mass spectrometry-based histopathologic examination of atherosclerotic lesions. *Atherosclerosis* **2011**, *217*, 427−432.
(12) Martin-Lorenzo, M.; Alvarez-Llamas, G.; McDonnell, L. A.; Vivanco, F. Molecular histology of arteries: mass spectrometry imaging as a novel ex vivo tool to investigate atherosclerosis. *Expert Rev. Proteomics* **2016**, *13*, 69−81.
(13) Niedermeyer, T. H. J.; Strohalm, M. mMass as a Software Tool for the Annotation of Cyclic Peptide Tandem Mass Spectra. *Planta Med.* **2012**, *78*, 7.
(14) Emini Veseli, B.; Perrotta, P.; De Meyer, G. R. A.; Roth, L.; Van der Donckt, C.; Martinet, W.; De Meyer, G. R. Y. Animal models of atherosclerosis. *Eur. J. Pharmacol.* **2017**, *816*, 3−13.
(15) Diehl, P.; Nienaber, F.; Zaldivia, M. T. K.; Stamm, J.; Siegel, P. M.; Mellett, N. A.; Wessinger, M.; Wang, X. W.; McFadyen, J. D.; Bassler, N.; Puetz, G.; Htun, N. M.; Braig, D.; Habersberger, J.; Helbing, T.; Eisenhardt, S. U.; Fuller, M.; Bode, C.; Meikle, P. J.; Chen, Y. C.; Peter, K. Lysophosphatidylcholine is a Major Component of Platelet Microvesicles Promoting Platelet Activation and Reporting Atherosclerotic Plaque Instability. *Thromb. Haemostasis* **2019**, *119*, 1295−1310.
(16) Li, Y. F.; Li, R. S.; Samuel, S. B.; Cueto, R.; Li, X. Y.; Wang, H.; Yang, X. F. Lysophospholipids and their G protein-coupled receptors in atherosclerosis. *Front. Biosci., Landmark Ed.* **2016**, *21*, 70−88.
(17) Schmitz, G.; Ruebsaamen, K. Metabolism and atherogenic disease association of lysophosphatidylcholine. *Atherosclerosis* **2010**, *208*, 10−18.
(18) Wurtz, P.; Havulinna, A. S.; Soininen, P.; Tynkkynen, T.; Prieto-Merino, D.; Tillin, T.; Ghorbani, A.; Artati, A.; Wang, Q.; Tiainen, M.; Kangas, A. J.; Kettunen, J.; Kaikkonen, J.; Mikkila, V.; Jula, A.; Kahonen, M.; Lehtimaki, T.; Lawlor, D. A.; Gaunt, T. R.; Hughes, A. D.; Sattar, N.; Illig, T.; Adamski, J.; Wang, T. J.; Perola, M.; Ripatti, S.; Vasan, R. S.; Raitakari, O. T.; Gerszten, R. E.; Casas, J. P.; Chaturvedi, N.; Ala-Korpela, M.; Salomaa, V. Metabolite profiling and cardiovascular event risk: a prospective study of 3 population-based cohorts. *Circulation* **2015**, *131*, 774−785.
(19) Kohno, S.; Keenan, A. L.; Ntambi, J. M.; Miyazaki, M. Lipidomic insight into cardiovascular diseases. *Biochem. Biophys. Res. Commun.* **2018**, *504*, 590−595.
(20) Stegemann, C.; Pechlaner, R.; Willeit, P.; Langley, S. R.; Mangino, M.; Mayr, U.; Menni, C.; Moayyeri, A.; Santer, P.; Rungger, G.; Spector, T. D.; Willeit, J.; Kiechl, S.; Mayr, M. Lipidomics Profiling and Risk of Cardiovascular Disease in the Prospective Population-Based Bruneck Study. *Circulation* **2014**, *129*, 1821−1831.
(21) Djekic, D.; Pinto, R.; Repsilber, D.; Hyotylainen, T.; Henein, M. Serum untargeted lipidomic profiling reveals dysfunction of phospholipid metabolism in subclinical coronary artery disease. *Vasc. Health Risk Manage.* **2019**, *15*, 123−135.
(22) Ward-Caviness, C. K.; Xu, T.; Aspelund, T.; Thorand, B.; Montrone, C.; Meisinger, C.; Dunger-Kaltenbach, I.; Zierer, A.; Yu, Z.; Helgadottir, I. R.; Harris, T. B.; Launer, L. J.; Ganna, A.; Lind, L.; Eiriksdottir, G.; Waldenberger, M.; Prehn, C.; Suhre, K.; Illig, T.; Adamski, J.; Ruepp, A.; Koenig, W.; Gudnason, V.; Emilsson, V.; Wang-Sattler, R.; Peters, A. Improvement of myocardial infarction risk prediction via inflammation-associated metabolite biomarkers. *Heart* **2017**, *103*, 1278−1285.
(23) Bot, M.; de Jager, S. C. A.; MacAleese, L.; Lagraauw, H. M.; van Berkel, T. J. C.; Quax, P. H. A.; Kuiper, J.; Heeren, R. M. A.; Biessen,

E. A. L.; Bot, I. Lysophosphatidic acid triggers mast cell-driven atherosclerotic plaque destabilization by increasing vascular inflammation. *J. Lipid Res.* **2013**, *54*, 1265−1274.
(24) Bot, M.; Bot, I.; Lopez-Vales, R.; van de Lest, C. N. A.; Saulnier-Blache, J. S.; Helms, J. B.; David, S.; van Berkel, T. J. C.; Biessen, E. A. L. Atherosclerotic Lesion Progression Changes Lysophosphatidic Acid Homeostasis to Favor its Accumulation. *Am. J. Pathol.* **2010**, *176*, 3073−3084.
(25) Kurano, M.; Suzuki, A.; Inoue, A.; Tokuhara, Y.; Kano, K.; Matsumoto, H.; Igarashi, K.; Ohkawa, R.; Nakamura, K.; Dohi, T.; Miyauchi, K.; Daida, H.; Tsukamoto, K.; Ikeda, H.; Aoki, J.; Yatomi, Y. Possible Involvement of Minor Lysophospholipids in the Increase in Plasma Lysophosphatidic Acid in Acute Coronary Syndrome. *Arterioscler., Thromb., Vasc. Biol.* **2015**, *35*, 463−470.
(26) Spector, A. A. Plaque rupture, lysophosphatidic acid, and thrombosis. *Circulation* **2003**, *108*, 641−643.
(27) Bot, M.; Nofer, J. R.; van Berkel, T. J. C.; Biessen, E. A. L. Lysophospholipids: two-faced mediators in atherosclerosis. *Future Lipidol.* **2007**, *2*, 341−356.
(28) Robertson-Gray, O. J.; Walsh, S. K.; Ryberg, E.; Jonsson-Rylander, A. C.; Lipina, C.; Wainwright, C. L. l-alpha-Lysophosphatidylinositol (LPI) aggravates myocardial ischemia/reperfusion injury via a GPR55/ROCK-dependent pathway. *Pharmacol. Res. Perspect.* **2019**, *7*, No. e00487.
(29) Kikuchiyanoshita, R.; Yanoshita, R.; Kudo, I.; Arai, H.; Takamura, T.; Nomoto, K.; Inoue, K. Preferential Hydrolysis of Phosphatidylethanolamine in Rat Ischemic Heart Homogenates during in-Vitro Incubation. *J. Biochem.* **1993**, *114*, 33−38.
(30) Law, S. H.; Chan, M. L.; Marathe, G. K.; Parveen, F.; Chen, C. H.; Ke, L. Y. An Updated Review of Lysophosphatidylcholine Metabolism in Human Diseases. *Int. J. Mol. Sci.* **2019**, *20*, 1149.
(31) Lehti, S.; Sjovall, P.; Kakela, R.; Mayranpaa, M. I.; Kovanen, P. T.; Oorni, K. Spatial distributions of lipids in atherosclerosis of human coronary arteries studied by time-of-flight secondary ion mass spectrometry. *Am. J. Pathol.* **2015**, *185*, 1216−1233.
(32) Schlitt, A.; Blankenberg, S.; Yan, D. G.; von Gizycki, H.; Buerke, M.; Werdan, K.; Bickel, C.; Lackner, K. J.; Meyer, J.; Rupprecht, H. J.; Jiang, X. C. Further evaluation of plasma sphingomyelin levels as a risk factor for coronary artery disease. *Nutr. Metab.* **2006**, *3*, 5.
(33) Jiang, X. C.; Paultre, F.; Pearson, T. A.; Reed, R. G.; Francis, C. K.; Lin, M.; Berglund, L.; Tall, A. R. Plasma sphingomyelin level as a risk factor for coronary artery disease. *Arterioscler., Thromb., Vasc. Biol.* **2000**, *20*, 2614−2618.
(34) Li, Z. Q.; Basterr, M. J.; Hailemariam, T. K.; Hojjati, M. R.; Lu, S. D.; Liu, J.; Liu, R. J.; Zhou, H. W.; Jiang, X. C. The effect of dietary sphingolipids on plasma sphingomyelin metabolism and atherosclerosis. *Biochim. Biophys. Acta, Mol. Cell Biol. Lipids* **2005**, *1735*, 130−134.

https://dx.doi.org/10.1021/jasms.0c00070
J. Am. Soc. Mass Spectrom. 2020, 31, 1825−1832